

XMaS **2018**

NEWSLETTER

CONTENTS

- 2 | XMaS Phase V
- 3 | XMaS Upgrade
- 5 | Technical Developments
- 6 | Condensed Matter
- 9 | Healthcare
- 10 | Soft Matter
- 12 | Materials Science
- 14 | Energy & Catalysis
- 16 | Access to offline facilities



On the cover: simultaneous GI-WAXS and opto-electrical measurements during *in-situ* annealing of a perovskite solar cell (p.12).

[1] www.xmas.ac.uk/impact/publications/

[2] www.aps.anl.gov/Beamlines/Directory

[3] www.xmas.ac.uk/impact/xmas_scientist_experience/

[4] www.esrf.eu/home/education/synchrotronschool.html

[5] www.thegazette.co.uk/notice/2937702

[6] www.iop.org/about/awards/president/medallists/page_72370.html

XMaS Phase V

It is with great pleasure we can announce that EPSRC has approved funding for XMaS to continue until the autumn of 2023. The next 2 years will see a total refurbishment of the beamline, since operation started in 1997, and will include an upgrade of the optics and the diffractometer to take advantage of the new ESRF-EBS source - further details are contained herein. We would like to thank everybody who was involved in preparing the scientific case and value your continuing support into the future.

There are some important changes both to the managerial structure and operational support of the facility. Dr. Yvonne Gründer from the University of Liverpool becomes a co-director of the project with a specific role in overseeing impact activities. As part of the new funding, we have secured additional resources to help users to accelerate the impact that results from their work, please contact us for more information. Two new post-doctoral positions will become available when user operations recommence in late 2020. Dr. Simon Brown, after over 20 years of service to the beamline, has taken early retirement and we would like to thank him for his enormous contribution to the project, ranging from the early stages of design and commissioning, to the maturation of the beamline into a reliable and innovative user facility. We all wish him well with his future plans.

The output of the beamline continues to grow both in volume and impact: 2018 was a record year! We recorded the highest number of publications in a single year (27) of which a record number (10) were published in high impact journals. A complete list of publications is maintained on the XMaS webpage; please explore the list to see the range and quality of the outputs [1]. If there are publications missing which contain XMaS work, please let us know.

In preparation for the EBS upgrade, XMaS was unavailable for the summer of 2018 as the experimental lead hutch was extended to preserve a good focusing and minimise aberrations. The official 20 month EBS upgrade started on Monday 10th December 2018. You will see in later pages, we are well advanced in our planning for the start up in 2020 with a completely revamped beamline to take advantage of the new EBS source.

During the upgrade period (which officially ends in August 2020), the offline Cu microsource is available for use and users are encouraged to apply for time. Many of the cryostats and sample environments can be used for offline measurements. Please get in touch with the beamline team for more details. In a strategic partnership with the APS, we have some T&S resources to support successful applications to the APS general users program (GUP) [2]. Further details are available on our website.

We anticipate holding an XMaS User meeting during 2019 to present the enhanced capabilities and capacity of the beamline. A user proposal round will open in March 2020 for the ESRF public allocation and April 2020 for direct CRG access. We look forward to receiving your applications and re-starting user operations. As a consequence of GDPR regulations, we asked users whether they wished to continue to receive information about the beamline. If you did not reply, you would have been removed from our database. If you wish to be added and continue to receive updates, please get in touch.

The annual XMaS Scientist Experience [3], where female A level Physics students from the UK take part in the ESRF's Synchrotron@schools [4] program and visit the beamline, will continue in 2019. We thank the ESRF staff for their help in making this activity so successful. Finally, Prof. Bill Stirling one of the original directors of XMaS, was awarded the Companion of the Order of St Michael and St George for services to British science and international science collaboration in December 2017 [5]. This was followed by the award in November 2018 of the Institute of Physics President's Medal [6]. Everyone associated with the beamline congratulates Bill on these well-earned, prestigious awards.

Chris Lucas, Yvonne Gründer, Tom Hase and Malcolm Cooper



XMaS Upgrade during 2018

Fig. 1: Panoramic view of the new control cabin.

December 10th 2018 08:00 was a benchmark in the ESRF history as it marked the end of 30 years of science using the first third-generation storage ring. It also coincided with the start of construction of a new machine that will provide the most brilliant x-ray beam in the world in 2020. The so-called *Extremely Brilliant Source* (EBS) [1] will be the first high-energy fourth generation synchrotron.

We started major upgrades to the XMaS beamline before the 20-month EBS shutdown began. Mid-May 2018, the diffractometer was craned out of the hutch only a few hours after the last experiment finished. It was the first time in twenty years! Pictures of our flying diffractometer are available on [Twitter](#) (@XMaSBeam #XMaSupgrade). Once all the equipment were secured, the beamline subsequently became a building site for four months. The control cabin was first dismantled leaving a huge empty space and direct access to the nearby beamline ID29. Our neighbours were actually pleased by this sudden increase of field of view but it obviously could not last. The experimental hutch (EH1) extension was completed in three weeks. Then the new control cabin was constructed (Fig. 1) followed by the installation of the electricity, fluids, air extraction and conditioning, etc... We were allowed to take beam again on September 27th. The Safety group checked that the new EH1 was white beam proof and it was!

The remaining few weeks of beam before the start of the EBS shutdown were spent testing the efficiency of our cryogenically cooled Si(111)

monochromator that we installed two weeks before taking beam again (Fig. 2). The subsequent reduction of heat load on the first crystal improved the quality of the monochromatic beam impinging on the sample. The spot size at the sample position is now 300 μm x 300 μm (800 μm (V) x 300 μm (H) before) and will be further reduced after the installation of the new mirror (see p. 4 for more details).

The operational energy of the new monochromator now ranges between 2.1 and 41 keV. The energy cut-off of the new toroidal mirror system will be 33 keV after the upgrade.

The mechanical stability of the monochromator system was tested down to 2.1 keV corresponding to a monochromator angle of $\sim 70^\circ$ (see Fig. 2). More design work was added to the original project to overcome the problem of side load affecting the actuators at these large angles. The cooling of the whole assembly is now done by means of copper (spiral) tubes, giving more flexibility during mounting, thus considerably reducing the torque.

Both sides of the energy spectrum accessible by the liquid nitrogen (LN_2) cooled monochromator were tested before the start of the EBS shutdown. X-ray Absorption Spectroscopy (XAS) spectra were measured across the phosphorus K-edge (2.14 keV). For the upper energy spectrum, the longer Si crystals and the mechanical design of the LN_2 monochromator now allow 41 keV to be reached, i.e. just above the cerium K-edge (40.44 keV). The flux is however, limited by the energy cut-off of the toroidal mirror. This

cut-off will be increased from 15 keV to 33 keV with the new system (see next page for mirror specifications). Improvements to the data statistics will be addressed during the ESRF dark period (e.g. acquisition of a multi-element detector with higher dynamic range and faster counting chain electronics).

The versatility of our diffractometer has always been an asset to the beamline for trying specific setups for novel experiments. Our CRG colleagues from BM20 (ROBL) [2] took advantage of our crystal analyser mount and energy dispersive detector to perform High Energy Resolution Fluorescence Detection (HERFD) using a large curved analyser crystal. See the article by K. Kvashnina *et al.*, p. 5 for more details. The quality of the results compared to conventional XAS combined with the low energy photons available on XMaS open up new opportunities for chemists from 2020, when the beamline re-opens.

[1] www.esrf.eu/about/upgrade

[2] www.hzdr.de/db/Cms?pNid=247

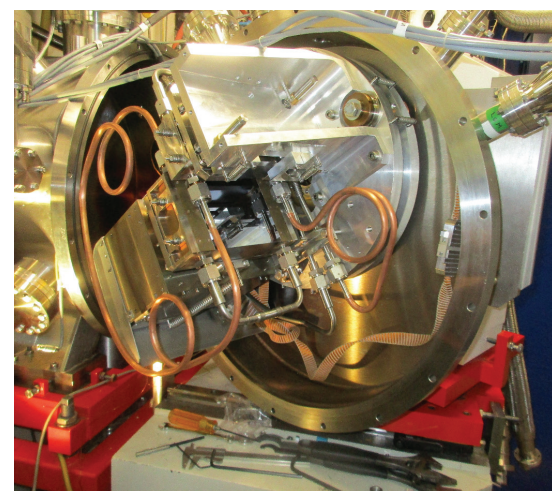


Fig. 2: LN_2 cooled monochromator photographed before closing the chamber.

XMaS 2019-2020

It has now been a few weeks since the last users deserted the experimental hall. Most of the activities have now concentrated on the machine side. The ESRF staff have twenty months to dismantle the old storage ring, install and test the new one. The injection of the first electrons in the EBS ring is planned for 2nd December 2019. The commissioning of the first ESRF beamlines will start in March 2020. The small ‘short-bend’ (SB) magnet that will replace the old BM28 bending magnet, will be installed in June 2020. We are planning to be back to user operation in the following autumn. Meanwhile, we are upgrading the whole XMaS beamline starting from the front-end (FE) right up to the detector position (see the *2017 XMaS Newsletter* [1] for a more detailed summary of the upgrade plan).

One major impact of the EBS project affecting XMaS is the position of the x-ray source point, which will move upstream by some 2.76 m. This implies moving the diffractometer downstream by an equal amount to preserve the current focusing and minimise aberrations: this in turn has necessitated the extension of the experimental hutch by several metres (see p. 3 for more details). The second constraint is that the x-ray beam will also move closer to the storage ring: 10 cm at the FE and ~20 cm at the new diffractometer position. Thus,

all equipment (slits, monochromator, mirror, etc...) and vacuum tubes must be moved sideways and lead panels need modifying to accommodate the new position of the beam. The displacement of the equipment is scheduled early summer 2019 and is conditioned by the availability of the ESRF overhead cranes heavily used for the machine construction. In the meantime, the infrastructure work needed to modify the sample preparation laboratory entrance and exit walls for the vacuum tubes is ongoing.

We are planning to re-use as much equipment (slits, tables, vacuum chambers, shutter) as possible. Some beam positioning diagnostics (e.g. beam position monitors) and conditioning (e.g. beam absorber) will be added in the optics (OH1) and experimental hutches (EH1). The monochromator and focusing mirror will move downstream. The new layout of OH1 is being finalised. The new toroidal mirror project is on schedule. The mirror assembly will consist of two interchangeable, meridionally bendable, cylindrical Si blocks coated with Cr and Pt, respectively, thereby increasing the working cut-off energy up to 33 keV (Fig. 3). On top of having better quality mirrors (roughness, smaller slope errors and new coatings), flux will be further gained by having longer substrates than before. Experiments beyond 33 keV will be possible but with reduced flux. The local company IRELEC [2] that

won the bid for the tender is now preparing the final design report and has already ordered the Si substrates. The mirror delivery is planned for December 2019. The recent installation of our LN₂ cooled monochromator has been tested to an upper energy of 41 keV (see p. 3 for more details).

The lead thickness of both OH1 and EH1 was specified back in 1995 to allow experiments to be performed using the white beam with a 0.4 Tesla bending magnet as a source. As the new SB source will have a magnetic field of 0.85 Tesla, the critical energy of the beamline is roughly doubling, hence the thickness of the lead in EH1 is unfortunately not sufficient for a white beam to be used from 2020. However, the new EH1 beam delivery system is being designed such that white beam operation may still be possible in the future.

After twenty years of extensive operation, the diffractometer will shortly be shipped back to Huber Diffraktionstechnik GmbH [3] for refurbishment and modifications of the 2 Θ arm. The new 2 Θ arm will accommodate two rails, one to mount point detectors (APD, silicon drift diode) and a light 2D detector (e.g. Maxipix) permanently thus allowing rapid switching between them; the polarisation analyser or larger 2D detectors (Pilatus) would be mounted on the second rail. The new design will also allow room for a high resolution analyser e.g. for HERFD experiment (see article in p. 5).

Finally, the long shutdown is also an opportunity to upgrade the old stepper motor drivers (DPAPs) to the latest ESRF standards (ICEPAPS). The DPAPs were already transferred inside EH1 during the hutch extension making the new control cabin a remarkably quieter and therefore more comfortable work area than before. We will replace the DPAPs (over 100!) with ICEPAPS, configure and test them one by one starting with the OH1 motors in the coming few weeks.

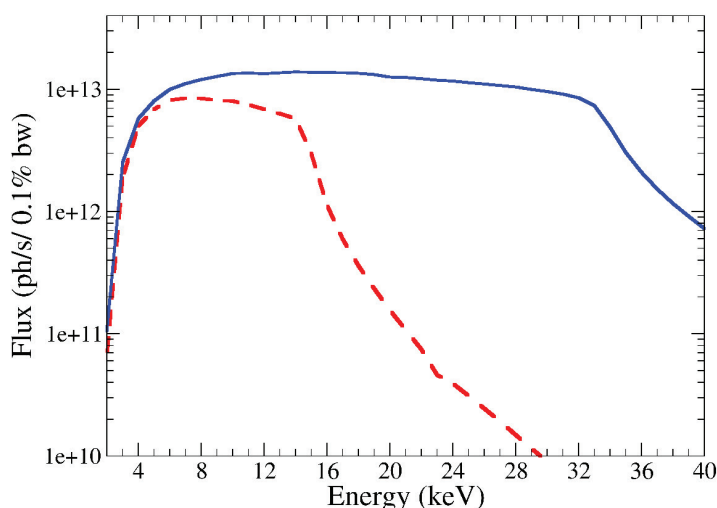


Fig. 3: Flux calculated at the sample position for a 100 x 100 μm^2 beam for the current (red) and new (blue) source assuming realistic parameters for the mirror aberrations and corrected for absorption.

- [1] www.xmas.ac.uk/impact/newsletters/
 [2] www.irelec-alcen.com
 [3] www.xhuber.de

X-ray Emission Spectrometer at the XMaS Beamline

K.O. Kvashnina, S. Bauters, L. Amidani, E. Gerber, I. Pidchenko and P. Thompson

An x-ray emission spectrometer has been installed recently at the XMaS beamline. The instrument has been tested in the hard and tender x-ray regions. The spectrometer provides possibility to study the electronic structure of matter by methods known as High Energy Resolution Fluorescence Detection (HERFD), X-ray Absorption Spectroscopy (XAS), X-ray Emission Spectroscopy (XES) and Resonant Inelastic X-ray Scattering (RIXS) [1,2].

The electronic structure information is very important and is related to different types of experiments such as diffraction, scattering, imaging etc. Nowadays, synchrotron users need to study systems with different techniques. Here we show the simple x-ray emission spectrometer setup installed on the XMaS diffractometer and tested in different energy ranges (Fig. 4). The spectrometer consists of a single spherically bent analyser and a detector placed on the 0.5 m diameter vertical Rowland circle. The HERFD, XES and RIXS spectra were recorded across the Ti K-edge (~ 4966 eV), Sb L_1 -edge (~ 4698 eV) and Bi M_5 -edge (~ 2580 eV).

The advantage of such a setup is that XAS spectra can be recorded with substantially better energy

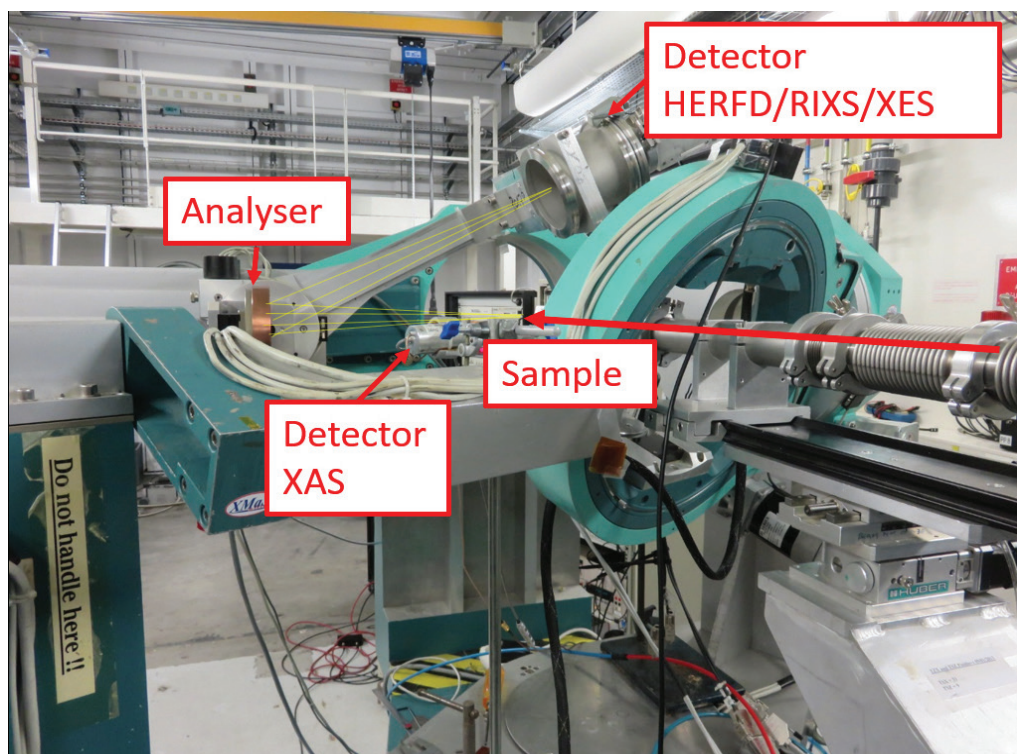


Fig. 4: Photograph of the x-ray emission spectrometer setup at XMaS.

resolution since the spectral broadening of the absorption features is drastically reduced in case of the HERFD detection method [3,4]. One example is shown in Fig. 5, where direct comparison between conventional XAS and HERFD data of CeO_2 at the Ce L_3 -edge is clearly demonstrated [5]. Addition of the crystal analyser to the spectrometer

setup also reduces the background generated by the other elements present in the investigated systems. Thus, the low detection limit of the elements of interest is substantially decreased even in complex materials.

XES and RIXS open up new opportunities to study valence and core x-ray emission lines in fine details. Thus those methods - HERFD, XES and RIXS - have a great potential in investigations of matter at the atomic and molecular scales.

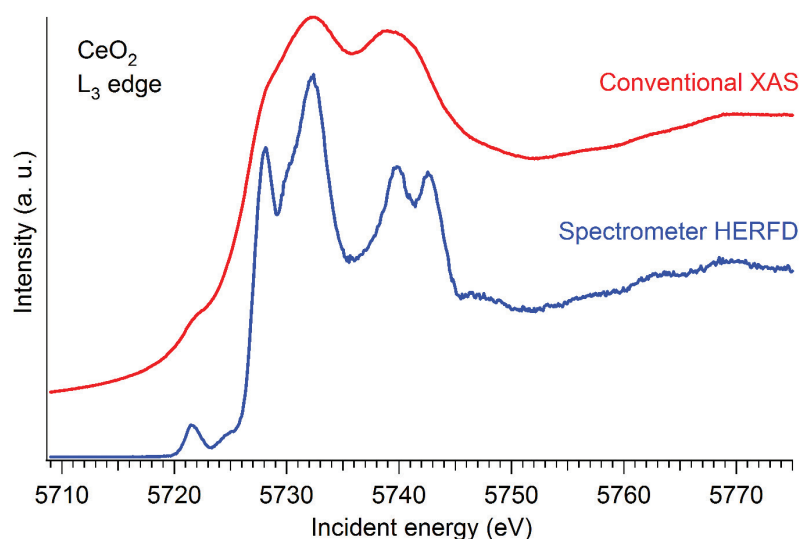


Fig. 5: Ce L_3 edge x-ray absorption spectra of CeO_2 recorded in HERFD mode (blue) by the x-ray emission spectrometer and in conventional XAS mode (red) by an avalanche photodiode.

- [1] K.O. Kvashnina, A.C. Scheinost, *J. Synchrotron Rad.* 23, 836 (2016).
- [2] P. Glatzel *et al.*, *J. Electron Spectros. Relat. Phenomena* 188, 17 (2013).
- [3] F. de Groot, A. Kotani, *Core Level Spectroscopy of Solids*, CRC Press (2008).
- [4] K. Hämäläinen *et al.*, *Phys. Rev. Lett.* 67, 2850 (1991).
- [5] K.O. Kvashnina *et al.*, *J. Anal. At. Spectrom.* 26, 1265 (2011).

For more information contact:
K.O. Kvashnina,
Rossendorf Beamline (ROBLE-CRG),
ESRF, Grenoble, France.
kristina.kvashnina@esrf.fr

Picometer polar atomic displacements in SrTiO₃ determined by resonant x-ray diffraction

C. Richter, M. Nentwich, M. Zschornak, E. Mehner, J. Hanzig, S. Gorfman, D.V. Novikov, D.C. Meyer

The physical properties of a crystal are strongly linked to the symmetry and variation of the atomic positions inside it. The displacement of atoms subjected to an external stimulus determines the response of the crystal or can lower the symmetry allowing for new properties to arise. Recently, we introduced a new approach of *Resonant X-ray Diffraction* (RXD) that yields to an enormous resonance contrast providing sensitivity to atomic displacements below the picometer scale [1]. The technique makes use of strong fluctuations in the atomic scattering amplitudes when the x-ray energy is scanned through an absorption edge. Potentially, these result in a sudden drop of intensity at an energy value that strongly depends on the atomic positions, but not on strain, providing access to minute thermal or static displacements.

We developed this approach with the aim to characterise structural changes in single crystals of strontium titanate (SrTiO₃) that have been predicted to take place during long-term application of an electric

field. In this situation, a strained surface layer develops at the anode side of the crystal. This process is referred to as electro-formation and has been attributed to the migration of oxygen vacancies [2]. In subsequent experiments, new physical properties have been observed in this layer, such as piezo- [3] and pyro-electricity [4], which cannot appear in normally cubic SrTiO₃. Hence, it is clear that a new low-symmetry phase has been stabilised in the electric field involving polar atomic displacements. This finding is important for the numerous applications of SrTiO₃ as a substrate or in semiconductor devices, but is also highly interesting as it may open another route for the development of lead-free piezo- and ferroelectrics.

Here, our specific goal was to characterise the interplay between strain and atomic displacements that vary in the sample throughout the strain gradient between the bulk and the polar SrTiO₃ layer.

The method we developed turned out to be ideal to study such problems.

Due to the strain gradient, the Bragg peaks coming from differently strained regions strongly overlap. By picking certain positions in the resulting, broad diffraction profiles, we can select certain strain states and study the corresponding atomic displacement via energy variation through the resonance. We found that sensitive Bragg reflections are those with exactly one odd Miller index, resulting in a counterplay of scattering contributions from the heavy strontium and the lighter titanium plus oxygen following the structure factor $F \approx f_{\text{Sr}} - f_{\text{O}} - f_{\text{Ti}}$.

To obtain accurate atomic positions, the dynamic thermal displacement needed to be refined in the first place. We did so for bulk SrTiO₃ by studying both temperature and energy dependence of the above mentioned reflections near the Sr *K* absorption edge. Based on that, we characterised the polar phase created after electro-formation using an electric field of 1 kV/mm⁻¹ applied along the [001] direction. The resulting distortion involves an elongation of the *c* parameter of up to 1%. Locally the symmetry is reduced to a polar tetragonal cell of space group *P4mm*. In addition to that, the energy dependencies revealed a shift of the Ti and O atoms along the *c* direction by ~ -1.3 pm and 3.7 pm, respectively (Fig. 6).

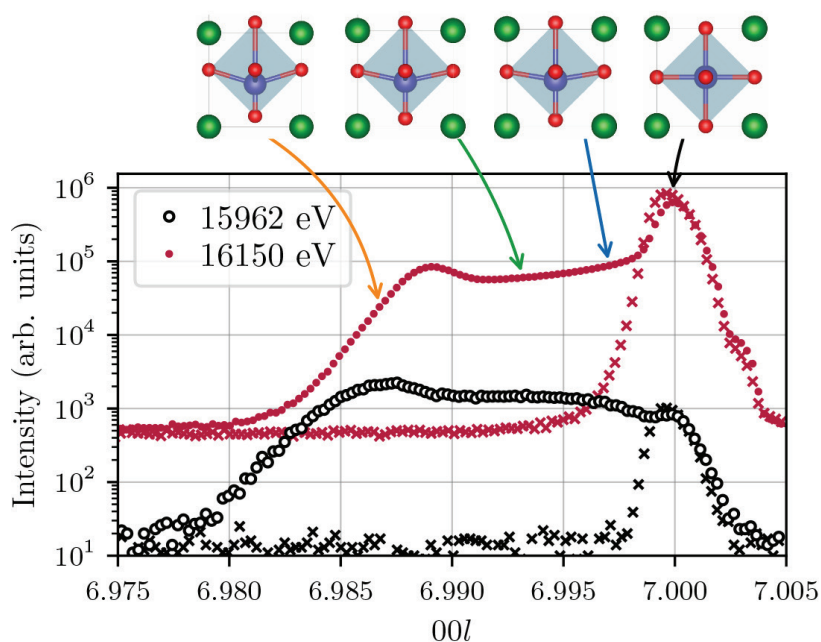


Fig. 6: The 007 reflection profile of SrTiO₃ before and after electro-formation and for two x-ray energies. Different positions in the scan relate to different magnitudes of strain and polar displacement as shown.

- [1] C. Richter *et al.*, Nat. Comm. 9, 178 (2018).
- [2] J. Hanzig *et al.*, Phys. Rev. B 88, 024104 (2013).
- [3] B. Khanbabaee *et al.*, Appl. Phys. Lett. 109, 222901 (2016).
- [4] J. Hanzig *et al.*, New J. Phys. 17, 023036 (2015).

For more information contact:
C. Richter, X-ray Nanoprobe Group,
ESRF, Grenoble, France.
carsten.richter@esrf.fr

Magnetostriction across the first order phase transition in Mn_2GaC MAX phase

Á.S. Ingason, T. Hase, R. Salikhov, M. Farle, J. Rosen *et al.*

MAX phases ($\text{M}_{n+1}\text{AX}_n$ with $n = 1, 2$ or 3) are laminated hexagonal compounds composed of the early transition metals M (Sc, Ti, V, Cr,...), A-group elements (Al, Ga, Ge,...) and X (C or N). These materials are interesting for potential technological applications as they have a high decomposition temperature, are resistant to oxidation and thermal shocks whilst being lightweight and elastically rigid. At the same time they are, like metals, good electric and thermal conductors. Thus, MAX phases can be viewed as a family of nano-laminated ceramics with high electrical and thermal conductivities.

In 2013, the new class of magnetic MAX phases was discovered [1]. Magnetic long-range order in these compounds is stabilised by substituting the M-element with Mn in ternary and quaternary compounds such as Mn_2GaC [2] (Fig. 7a) and $(\text{Cr}_{0.5}\text{Mn}_{0.5})_2\text{GaC}$ [3]. Such magnetic MAX phases have since become an exciting research field due to their possible exploitation in magnetic wear resistant coatings, magnetocalorics and spin transport applications. Mn_2GaC exhibits a high magnetic ordering temperature

(~ 507 K), a complex non-collinear temperature dependent magnetic behaviour and an anisotropic magnetostructural transformation at $T_T \sim 214$ K [4-5].

We studied the effect of an external magnetic field, B_a , on the structural properties of Mn_2GaC epitaxial films across this phase transition using high resolution double-axis diffraction and the XMaS 4 T superconducting magnet. The lattice parameter was determined from the (006) film peak as a function of B_a applied parallel to the film surface. At 200 K, the diffraction peak was observed to shift towards smaller scattering vectors $Q = |Q|$ as the field increases (Fig. 7b).

Above T_T , at 270 K, the opposite was seen, and the peaks moved to higher Q (Fig. 7b). Fig. 7c shows the relative change of the inter-plane distance Δd with respect to the d -spacing at zero field, d_0 , i.e. the magnetostriction. The magnetostriction is unchanged for applied fields below ~ 1 T. For higher fields, the magnetostriction strongly depends on the field strength and temperature.

Above T_T , the field induces an out-of-plane lattice compression which increases with B_a . At 200 K the magnetostriction changes sign, showing instead a tensile strain in response to B_a . Both c-axis magnetostrictions are large - about 450 ppm at 3 T (only four times smaller than the highest magnetostrictive material - Terfenol) [5].

We correlate these intriguing x-ray data with bulk structural and magnetisation measurements to elucidate the magnetic structure and find that above the transition temperature the system has an AFM spin configuration with a collinear spin alignment between the magnetic sub-lattices [4, 5]. At T_T the film undergoes a first order phase transition, characterised by the c-axis lattice compression accompanied by a concomitant spin transformation to a non-collinear state. This gives rise to the observed magnetostriction. The large magnitude and temperature dependent sign change of the magnetostriction may lead to new devices based on this new class of materials. Further details are described in [5].

- [1] A.S. Ingason, *et al.*, Phys. Rev. Lett. 110, 195502 (2013).
 [2] A.S. Ingason, *et al.*, Mater. Res. Lett. 2, 89 (2014).
 [3] A. Petruhins, *et al.*, J. Mater. Sci. 50, 4495 (2015).
 [4] M. Dahlvist, *et al.*, Phys. Rev. B 93, 014410 (2016).
 [5] I.P. Novoselova, *et al.*, Sci. Rep. 8, 2637 (2018).

*HAADF/STEM: High-Angle Annular Dark-Field Scanning Transmission Electron Microscopy

For more information contact:
 R. Salikhov, Faculty of Physics and
 Centre for Nanointegration (CENIDE),
 University of Duisburg-Essen,
 Duisburg, Germany.

ruslan.salikhov@uni-due.de

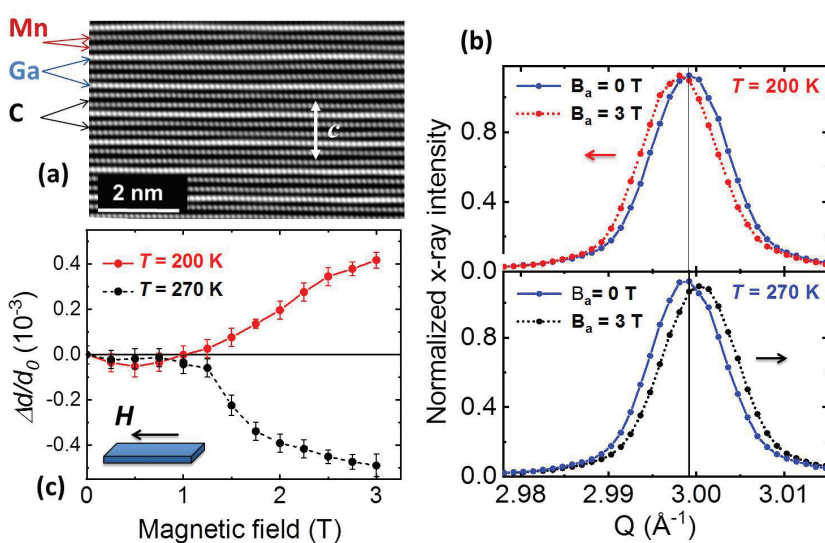


Fig. 7: (a) Cross-sectional HAADF/STEM* atomic resolution image of the Mn_2GaC film. The bright (grey) points correspond to Ga (Mn) atomic columns. (b) Comparison of the Mn_2GaC (006) x-ray diffraction peak for different magnetic fields and temperatures. (c) In-plane field dependence of magnetostriction measured at 200 K (red) and 270 K (dashed black).

Proximity-induced magnetism and Dzyaloshinskii-Moriya interaction at heavy metal/Co₂FeAl interfaces

A. Mora-Hernández, B. Nicholson, O.-O. Inyang, L. Bouchenoire, M. Belmeguenai, Y. Roussigné, H. Bouloussa, S.M. Chérif, A. Stashkevich, M. Nasui, M.S. Gabor, A.T. Hindmarch

Ultrathin film multilayers incorporating heavy-metal (HM) and ferromagnetic materials have many applications in the field of spintronics. At interfaces between these materials, due to the broken inversion symmetry, an interfacial Dzyaloshinskii-Moriya interaction (iDMI) arises. The iDMI is an antisymmetric exchange interaction which favours non-collinear alignment of neighbouring magnetic moments and results in chiral magnetic structures including domain-walls and skyrmions [1]. Details of the structure and magnetism at the interface play a crucial role in determining the iDMI [2].

Ferromagnetic Heusler alloys such as Co₂FeAl (CFA) possess high Curie temperatures, relatively high spin polarisation approaching 100% and extremely small dissipative damping of magnetisation precession, making them very attractive materials for spintronic devices based on current-driven manipulation of domain walls and skyrmions. In such alloys, there is always some degree of chemical disorder, which strongly influences many of their physical properties [3].

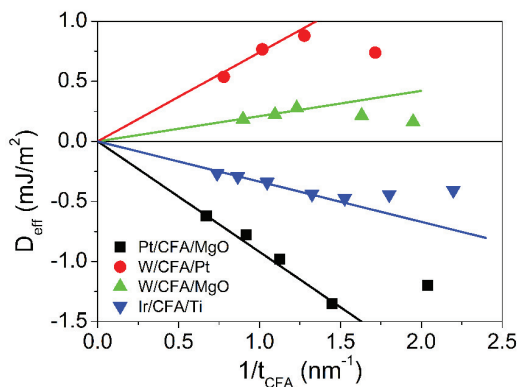


Fig. 8: Inverse CFA thickness dependence of the iDMI constant in several multilayer structures, measured by Brillouin light scattering. Deviation from expected linear behaviour for an interface effect is found at small CFA layer thicknesses, due to reduced CFA magnetisation.

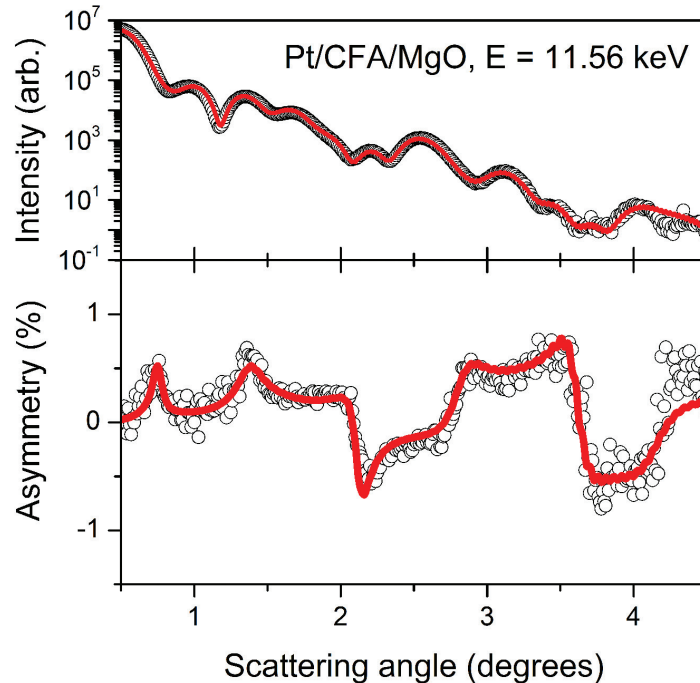


Fig. 9: XRMR (upper) and asymmetry (lower) for a Pt/CFA/MgO trilayer measured at the Pt L₃ absorption edge. Non-zero asymmetry demonstrates the presence of proximity-induced magnetism in Pt, which requires that the CFA layer is ferromagnetic at the Pt/CFA interface. The fits provide both structural information and the depth profile of proximity induced magnetism in the Pt layer.

Chemical disorder is likely to occur at interfaces; in our devices the few-nm thick CFA layer is sandwiched between HM (Pt or Ir) and insulating MgO layers. Brillouin light scattering allows the iDMI to be quantified. Fig. 8 shows the inverse-thickness dependence of the iDMI constant for different CFA trilayer structures. Magnetometry measurements show that there is a region associated with the interface(s) where the magnetisation is reduced, possibly to zero; this reduced interfacial magnetisation would have significant impact on spintronic device functionality and performance, modifying both interfacial spin-polarisation and iDMI.

Conventional magnetometry is unable to provide depth resolution, allowing only a volume averaged magnetisation to be determined. X-ray Resonant Magnetic Reflectivity (XRMR) enables depth- and element-

selective magnetometry. Tuning the x-ray energy to the L₃ absorption edge of HM, as in Fig. 9, provides sensitivity specifically to proximity-induced magnetism in the HM layer, which in turn provides indirect information on the magnetism in CFA at the CFA/HM interface [3].

This work is performed in collaboration with the Technical University of Cluj-Napoca, Romania, and Université Paris 13, France.

[1] A. Fert *et al.*, Nat. Nanotechnol. 8, 152 (2013).

[2] R.M. Rowan-Robinson *et al.*, Sc. Rep. 7, 16835 (2017).

[3] M. Belmeguenai *et al.*, Phys. Rev. Applied 9, 044044 (2018).

For more information contact:
A. T. Hindmarch,
Department of Physics,
Durham University, UK.

a.t.hindmarch@durham.ac.uk

Towards a spatial and temporal model of human enamel biomineralisation

M. Al-Mosawi, D.A. Montgomery, J. Beaumont, M. Al-Jawad

Human dental enamel biomineralisation is a phenomenon whose timings and spatial progression is poorly understood. For dental and skeletal tissue research, understanding organic matrix-mediated mineralisation holds the key to developing successful reparative or regenerative hard tissue biomimetic medical and dental technologies. Our aim was to use synchrotron X-Ray Diffraction (XRD) on human dental enamel

archaeological collection. Experimental details can be found in the published article [2].

XMT revealed a bi-directional mineralisation « front » starting vertically at the dentine horn tip and horizontally at the enamel-dentine junction (EDJ) travelling cervically and peripherally as a function of enamel maturation until the relative mineral density was uniform in the fully mature tooth at $2.75(1) \text{ g.cm}^{-3}$

percentage to the overall crystalline structure. These phenomena were observed in all stages of tooth development with the precise spatial distributions varying somewhat at each developmental stage. qBSE analyses suggested that the two observed populations are most likely due to spatial changes in crystallite bundle (prism) orientations (known as prism decussation), and revealed that mineralisation of prism cores precedes that of prism boundaries [2].

Quantification of the direction and magnitude of organisation within two distinct populations of crystallites in developing and mature enamel has not been shown previously. These results allow us to understand the development of the complex hierarchical structure within human enamel and provide new insights towards building a quantitative spatio-temporal model of human enamel biomineralisation.

[1] www.diamond.ac.uk/Instruments/Magnetic-Materials/B16.html

[2] M. Al-Mosawi *et al.*, *Sci. Rep.* 8, 14449 (2018).

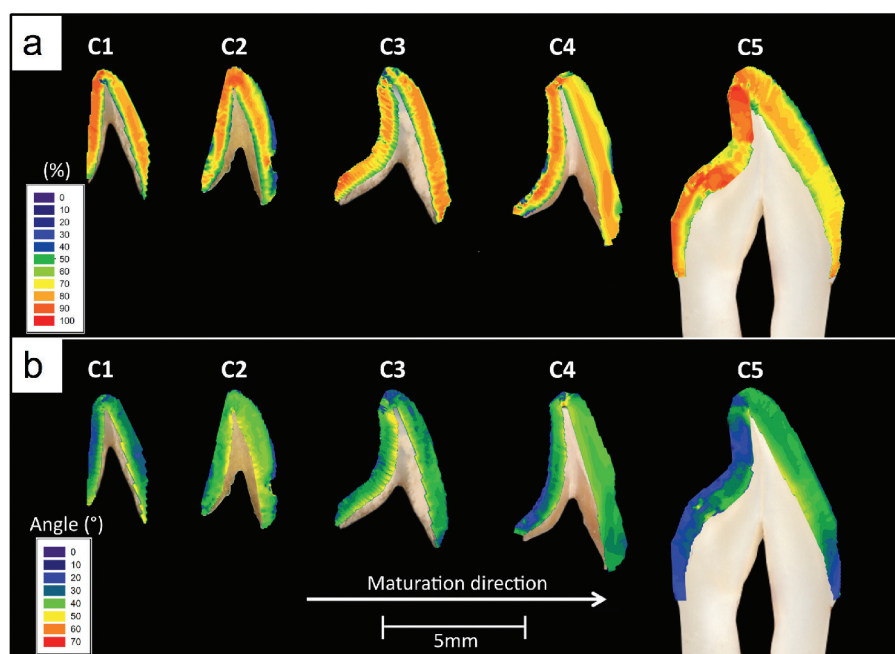


Fig. 10: (a) Percentage of crystallites belonging to the first orientation population and (b) the angle between the two orientation populations [2].

at different stages of development to provide novel insights into the biomineralisation process to inform emerging technologies in regenerative and reparative dentistry.

Synchrotron XRD using XMaS at the ESRF and B16 at DLS [1] combined with X-ray absorption Microtomography (XMT) and Quantitative Backscattered Electron (qBSE) imaging were used to generate crystallographic orientation, mineral density and micro-morphology maps of five human central incisors at different stages of enamel maturation taken from an

(not shown here but available in [2]). Analysing azimuthally 2D synchrotron XRD patterns revealed that within any probed region, two crystallite-orientation populations coexisted. One population contributed a higher percentage, by a factor of ~ 4 , to the overall crystalline structure (Fig. 10a). The angular separation between the two populations was $\sim 40^\circ$, varying as a function of position within the tooth crown (Fig. 10b). Interestingly, the population with a significantly lower texture magnitude (i.e. higher FWHM values in Fig. 11a compared to Fig. 11b) contributed to a higher

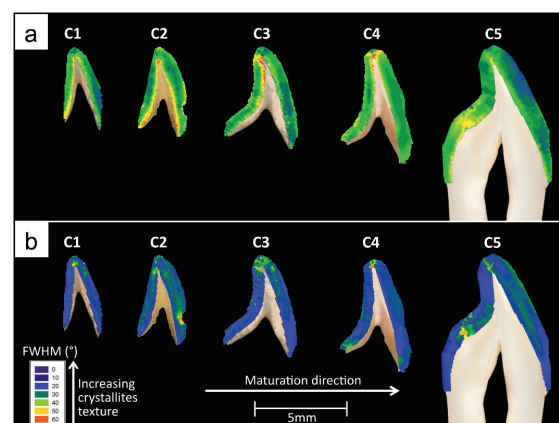


Fig. 11: Texture magnitude distribution of crystallites of (a) first and (b) second orientation populations [2].

For more information contact:
M. Al-Jawad, Institute of Dentistry,
Queen Mary, University of London, UK.
m.al-jawad@qmul.ac.uk

Trigonal columnar self-assembly of bent phasid mesogens

H.F. Cheng, Y.X. Li, X.B. Zeng, H.F. Gao, X.H. Cheng, G. Ungar

The term “phasid” mesogen is used to describe rod-like molecules with three flexible chains, usually alkyl, at each end. The name also refers to the similarity with the six-legged insects known by the same name. Usually such mesogens form the **hexagonal** columnar (Col_{hex}) liquid crystal (LC) phase, where aromatic rods form column cores, while the alkyls fill the space between the columns. The question is whether a **trigonal** columnar LC phase can be formed, with three-fold rather than six-fold symmetry and with non-cylindrical columns. Such non-centrosymmetric structures are rare in liquid crystals but are of interest for their potential ferroelectric, pyroelectric or nonlinear optical properties.

Here we show that columns with a three-arm star cross-section and trigonal symmetry can form from a series of compounds (Fig. 12a), with a bent rod-like aromatic core and three alkoxy chains at each end [1]. The columnar liquid crystal phase has a non-centrosymmetric trigonal *p31m* symmetry.

The $1/d^2$ values of the three XRD peaks observed for the phase are in the ratio 1:3:4, indicating a hexagonal or trigonal lattice. This

is clearly shown in the hexagonal symmetry of the 2D diffraction pattern of the phase, recorded by Grazing Incidence Small Angle X-ray Scattering (GISAXS) pattern on a surface oriented thin film at BM28, ESRF (Fig. 12b). In the thin film the columns are oriented parallel to the substrate surface (planar anchoring), rather than perpendicular to it.

The fact that the phase is not centrosymmetric is confirmed by the emission of Second Harmonic Generation (SHG) light. A pulsed laser at 800 nm was attached to the microscope and focused onto the sample resulting in a SHG signal detectable at 400 nm. Fig. 12c shows a large increase in SHG signal above the background level on cooling from isotropic to Col_{hex} phase, showing clearly that the latter phase lacks centre of symmetry and is thus a trigonal phase. The plane group of the phase is thus determined to be *p31m* instead of *p6mm*.

Geometry optimisation and molecular dynamic simulation were performed. A snapshot of molecular dynamic simulation is shown in Fig. 13a. We consider that the efficient back-to-back packing of the three bent cores in this structure is facilitated by a degree of flexibility

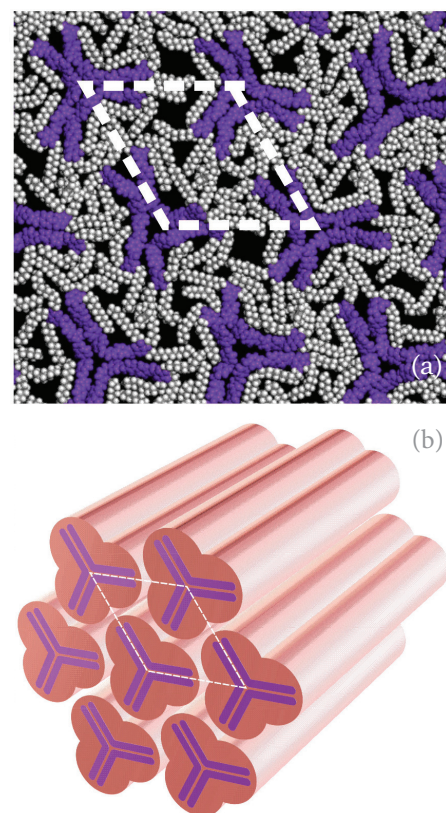


Fig. 13: (a) Snapshot of molecular dynamic simulation: purple = aromatic, grey and white = aliphatic chains. (b) Schematic of the Col_{hex}/*p31m* phase.

in the core, particularly around the oxymethylene linkage. The long-range polarity, on the other hand, is believed to be secured by the high barrier for uncorrelated rotation around the column axis. The schematic of the Col_{hex}/*p31m* phase is shown in Fig. 13b.

In summary, a series of bent-core phasid compounds were synthesized, capable of forming a trigonal columnar phase. Unlike any columnar LC phases previously discovered, the aromatic columns adopt an unusual 3-armed star-shaped cross-section. This finding indicates a potential new path to creating non-centrosymmetric self-assemblies that could, with suitable substituents, be used in ferroelectric, pyroelectric or frequency-doubling optical devices.

[1] H.F. Cheng *et al.*, Chem. Commun. 54, 156 (2018).

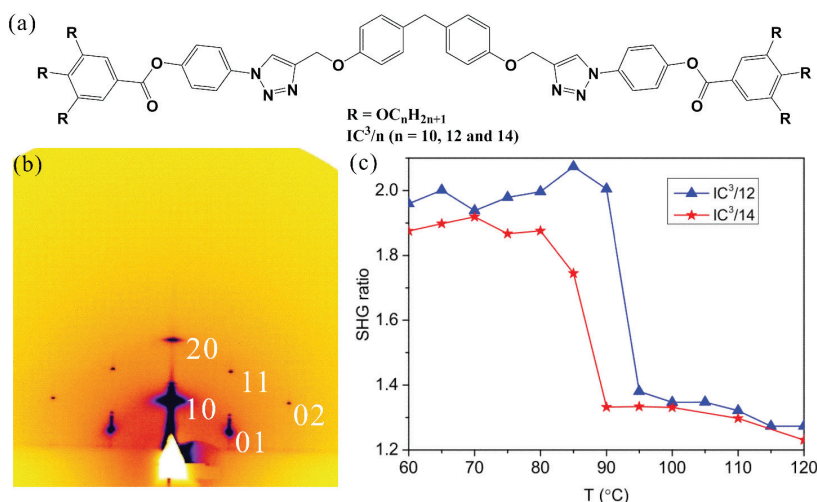


Fig. 12: (a) Chemical structure of bent phasid mesogens IC³/*n*. (b) GISAXS diffraction pattern of IC³/12 recorded at 80°C at BM28. (c) Temperature dependent intensity of the second harmonic (400 nm) vs background (800 nm excitation), generated 20 μm above the substrate surface in slow cooling.

For more information contact:
X.B. Zeng, Department of Materials
Science and Engineering,
University of Sheffield, UK.

x.zeng@sheffield.ac.uk

Surface structure of few layer graphene

L. Zhou, L. Fox, M. Włodek, L.I. Flores, A. Slastanova, E. Robles, O. Bikondoa, W.H. Briscoe

Graphene is a one-atom thick, flat, carbon monolayer with a hexagonal carbon aromatic structure. Since the first graphene sheet was successfully exfoliated by Novoselov and Geim, its unique (physical) properties have stimulated numerous research on potential applications in a range of technologies including supercapacitors and biosensors [1]. Previous studies have shown that the physical properties of graphene-related materials are determined by their structure, specifically the thickness [2] and any defects or contaminants [3]. Therefore, understanding the structure of graphene is important for its integration into new composite materials.

Different techniques, such as Atomic Force Microscopy (AFM) and Raman spectroscopy, have been employed for the structural characterisation of graphene. However, these techniques have a limited capacity to probe the out-of-plane structure of the adsorbed layer. Another powerful technique is X-ray Reflectivity (XRR), which is widely used for probing buried interfaces and thin films [4]. XRR has been used to study the exposed and buried interfacial structure of graphene grown on SiC [5], illustrating its potential for characterising the structure of graphene.

In our work, we used synchrotron XRR at the XMaS beamline [6] to determine the structure of commercially available graphene samples (prepared on SiO₂/Si via chemical vapour deposition and marketed as graphene monolayers) at different temperatures. X-ray photo-electron spectroscopy work function maps and AFM were employed to evaluate the composition and morphology of the samples. Our results (Fig. 14) indicate that the samples we characterised consisted of 3-4 layers of graphene, which should thus be more accurately described as few layer graphene (FLG). At 25°C, the FLG thickness from XRR was $13.0 \pm$

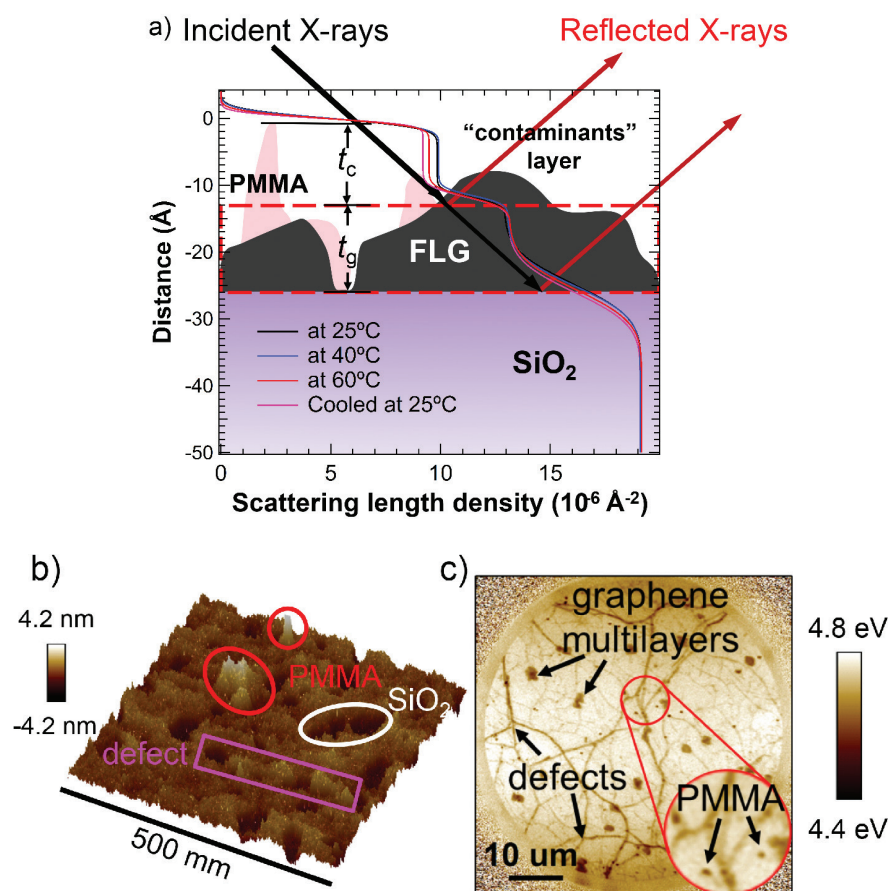


Fig. 14: (a) Fitted scattering length density profiles of the FLG at different temperatures with the corresponding physical model. Here, t_g and t_c are the thickness of the FLG and the contaminant slabs, respectively. (b) AFM 3D topological image of the FLG at room temperature. (c) The work function map of the FLG annealed at 450°C for 1 h.

1.0 \AA (mean thickness of 4 different samples from the same supplier), in agreement with that obtained from AFM ($13.9 \pm 0.7 \text{ \AA}$). Furthermore, a “contaminant” layer, comprising polymethylmethacrylate (PMMA) and graphene multilayers, was found atop the FLG layer.

A tentative effect of temperature on the FLG thickness has also been captured using XRR. Upon heating to 60°C, the FLG thickness expanded from 12.9 Å to 13.8 Å, which further increased to 14.3 Å upon cooling to 25°C. We attribute this temperature dependent thickness to the out-of-plane rippling of graphene, resulting from its negative in-plane thermal expansion coefficient, as previously reported [7]. More measurements are needed to further verify these interesting observations.

These unprecedented results on the FLG surface structure and chemistry are valuable to its potential bioanalytical applications.

- [1] K.S. Novoselov *et al.*, Nature 490, 192 (2012).
- [2] M.S. Xu *et al.*, ACS Nano 4, 2937 (2010).
- [3] C. Mattevi *et al.*, J. Mater. Chem. 21, 3324 (2011).
- [4] W.H. Briscoe *et al.*, Soft Matter 8, 5055 (2012).
- [5] M. Conrad *et al.*, Phys. Rev. B 96, 195304 (2017).
- [6] L. Zhou *et al.*, Carbon 136, 255 (2018).
- [7] D. Yoon *et al.*, Nano Lett. 11, 3227 (2011).

For more information contact:
W.H. Briscoe, School of Chemistry,
University of Bristol, UK.

wuge.briscoe@bristol.ac.uk

Clean semiconductor behaviour of perovskite solar cells probed by simultaneous current-voltage and GI-WAXS measurements

S. Lilliu, M. Alsari, O. Bikondoa *et al.*

Perovskite photovoltaics (PV) is one of the fastest growing optoelectronic technologies with device efficiencies currently exceeding 23% in single solar cells and 27.3% in tandem devices [1]. For most solution-processed perovskite materials, annealing temperature and duration are critical factors for optimised conversion of the as-coated precursor material into a functional polycrystalline perovskite film. In this work, Alsari and co-workers [2] employ a new investigation method illustrated in Fig. 15 that can significantly reduce the workload required in thermal engineering of perovskite solar cells and, at the same time, establish a direct correlation between their optoelectrical and structural properties during *in-situ* annealing. This is achieved by exploiting the concept of interdigitated back-contact (IBC) solar cells. Here the electron (TiO_2) and hole (PEDOT) selective electrodes are co-positioned on the backside of the cell in an interdigitated fashion (Fig. 15b) [3].

Because the perovskite film is unobstructed by any top layer, *in-situ* annealing can be performed without compromising the film formation. At

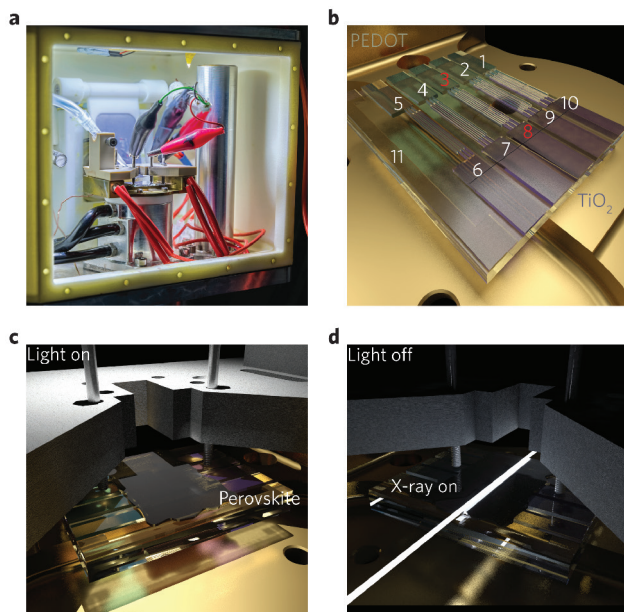


Fig. 15: Illustration of the measurements setup at XMaS [2].

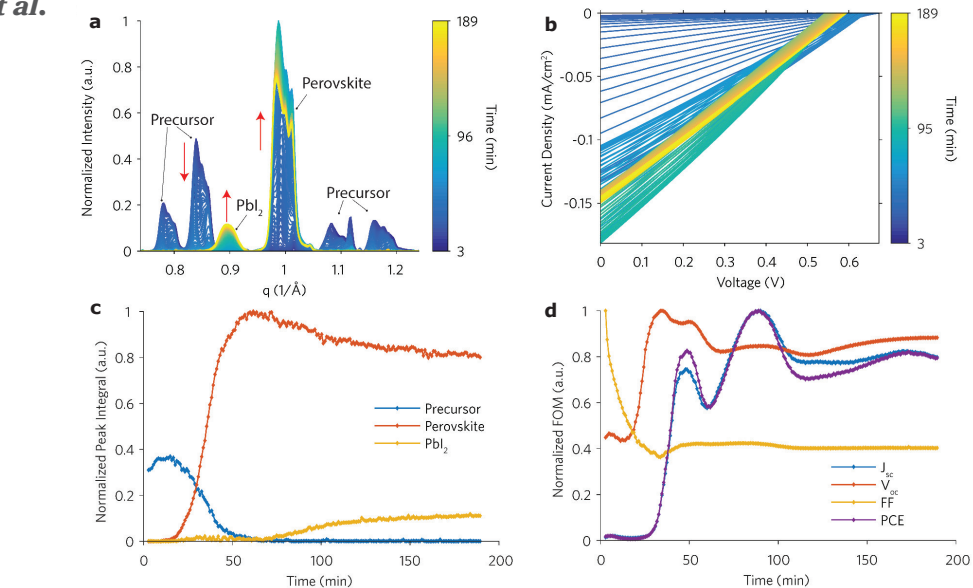


Fig. 16: Structural and opto-electrical parameters extracted from simultaneous GI-WAXS patterns (under dark conditions) and current-voltage (under light conditions) measurement of a perovskite ($\text{CH}_3\text{NH}_3\text{PbI}_3$) IBC solar cell during *in-situ* annealing at 88.2°C [2].

the same time, the perovskite film is directly accessible by an x-ray beam in Grazing Incidence Wide Angle X-ray Scattering (GI-WAXS) geometry. This makes IBC devices a great solution for simultaneous opto-electrical and GI-WAXS measurements performed *in-situ* during the annealing. With the setup developed at the XMaS beamline, Alsari *et al.* demonstrate a high throughput thermal engineering route that can be used on a variety of perovskite materials, along

with the possibility of establishing a direct correlation between the figures-of-merit of a solar cell and its structural properties. Fig. 16 shows a summary of the photovoltaic and structural measurements on $\text{CH}_3\text{NH}_3\text{PbI}_3$ perovskite IBC solar cells. The remarkably clean semiconductor behaviour of perovskites is evidenced by the high photovoltages measured at the first stages of perovskite conversion from precursors, at

the percolation threshold for bulk conductance. The open circuit voltage (V_{oc}) reaches a maximum value before the precursor has fully converted into perovskite, when the fraction of precursor and perovskite crystals is comparable (Fig. 16c-d). The short circuit current (J_{sc}) and power conversion efficiency (PCE) follow a trend similar to that of the perovskite peak intensity extracted from the GI-WAXS measurements.

The measurement strategy followed by Alsari *et al.* is not limited to perovskite materials and is of interest for any solution processable photovoltaic technology requiring thermal annealing.

- [1] H.J. Snaith and S. Lilliu, *SciVPro* 1, 1, (2018). doi:10.32386/scivpro.000004
 [2] M. Alsari *et al.*, *Energy Environ. Sci.* 11, 383 (2018).
 [3] L.M. Pazos-Outón *et al.*, *Science* 351, 1430 (2016).

For more information contact:
 S. Lilliu, Department of Physics and Astronomy, University of Sheffield, UK and The UAE Centre for Crystallography, United Arab Emirates.
 s.lilliu@sheffield.ac.uk

New tool for simulation of surface resonant x-ray diffraction

Y. Gründer, Y. Joly, Y. Soldo-Olivier

In-situ studies of the chemical bonding at an electrochemical interface are rather difficult due to the presence of the electrolyte and also because standard characterisation techniques which are mostly UHV based cannot be applied.

Surface X-ray Diffraction (SXRD) is widely used to solve the atomic structure at the surface of single crystals. One of its advantages is that it can be performed *in-situ* and even *operando*. On the other hand, X-ray Absorption Near Edge Spectroscopy (XANES) as well as Resonant X-ray Diffraction (RXRD) are highly sensitive to the oxidation states considering the edge energy shift compared to a known reference. Recording spectra across an absorption edge is possible on specific points of the crystal truncation rods (CTR), which are surface sensitive points in reciprocal space. As in 3D anomalous diffraction, spectra exhibit large intensity variations

around the edge. The so-called Surface Resonant X-ray Diffraction (SRXRD) is therefore expected to be sensitive to both the surface geometrical structure and the electronic structure around the absorbing elements. The existing fitting tool allows the description of the geometry but no one up to now was able to reproduce the spectra experimentally.

We have successfully employed SRXRD to gain site specific information about the charge distribution at a buried interface. Furthermore, the development of a theoretical tool based on an *ab-initio* approach further elucidated the charge transfer and bond formation at a polarised solid-liquid interface [1].

The calculation uses density functional theory to calculate the electronic structure around the resonant atoms. The atomic charges and the bonding with the

neighbouring atoms can then be deduced. With this information the modified form factors and thus energy and angular dependent resonant scattering amplitudes around the x-ray absorption edges can be modelled. For SRXRD, all contributions from the bulk and from the surface, which includes the substrate topmost atomic layers and the eventual adsorbed layers, are summed up and finally one obtains the intensity of the diffracted beams. It is the angular dependence of the surface alignment with the incoming x-ray beam, specifically the incoming beam polarisation, which shows that specific chemical bounds are probed.

We have demonstrated the validity of our approach studying different systems. As an example, we consider the formation of a bromine ad-layer on copper at an electrochemical interface. We show here the comparison of the simulated spectra with the data recorded at the XMaS beamline, across the Cu K-edge and along two polarisation directions of the incoming light (Fig. 17). The relative shift of these spectra versus references are related to the oxidation state of Cu. Furthermore, most of the features are signatures of the bonding with the neighbouring atoms. Because all the Cu atoms (i.e. bulk and surface) contribute, spectra recorded at different L values in reciprocal space must be analysed. Beyond this particular study, this work opens a new route to explore the electronic structure at surfaces and interfaces.

[1] Y. Joly *et al.*, J. Chem. Theory Comput. 14, 973 (2018).

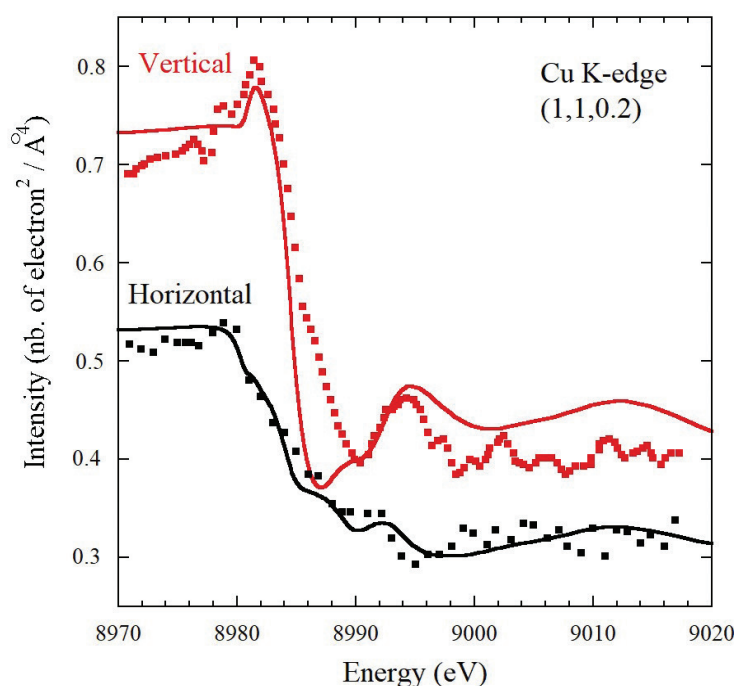


Fig. 17: Spectra at the Cu K-edge in the Br c(2x2) ad-layer on Cu(100) system recorded at XMaS (dots) for two polarisation directions with respect to the scattering plane, and compared with the simulations (lines).

For more information contact:
Y. Joly, Institut Néel, CNRS,
Grenoble, France.
yves.joly@neel.cnrs.fr

Probing the hydriding behaviour of a buried uranium interface with synchrotron radiation

J.E. Darnbrough, R.M. Harker, I. Griffiths, D. Wermeille, G.H. Lander and R. Springell

The safe, long term storage of metallic uranium samples requires a fundamental understanding and predictive capability regarding the uranium-hydrogen reaction [1]. The storage of metallic uranium in the presence of either moisture or organic materials in sealed containers is known to produce hydrogen over time. Hydrogen then goes on to react with uranium which, as described elsewhere, proceeds through four characteristic phases: induction, acceleration, linear and

β -UH₃ is formed between ambient temperatures and 100°C with the concentration of α -UH₃ increasing to significant proportions at room temperature and below [3]. This presents a significant safety hazard on opening the container to air, so knowing the amount of hydride produced allows a quantification of the hazard [4].

This article reports experiments investigating the reaction of H₂ with uranium metal-oxide bilayers [5].

either by deposition (via reactive magnetron sputtering) or allowing the uranium metal to oxidise in air at room temperature. The bilayers were exposed to hydrogen, with sample temperatures between 80 and 200°C, and monitored via *in-situ* X-ray Diffraction (XRD) (Fig. 18). Complementary experiments were also conducted using Scanning Transmission Electron Microscopy - Electron Energy Loss Spectroscopy (STEM-EELS) (Fig. 19).

Small partial pressures of H₂ caused rapid consumption of the U metal and lead to changes in the intensity and position of the diffraction peaks from both the UO₂ overlayers and the U metal. There is an orientational dependence in the rate of U consumption. From changes in the lattice parameter we deduce that hydrogen enters both the oxide and metal layers, contracting the oxide and expanding the metal. The air-grown oxide overlayers appear to hinder the H₂ reaction up to a threshold dose, but then on heating from 80 to 140°C, the consumption is more rapid than for the as-deposited overlayers. STEM-EELS establishes that the U-hydride layer lies at the oxide-metal interface. It also shows that the initial formation is at defects or grain boundaries and involves the formation of amorphous and/or nanocrystalline UH₃. This explains why no diffraction peaks from UH₃ are observed.

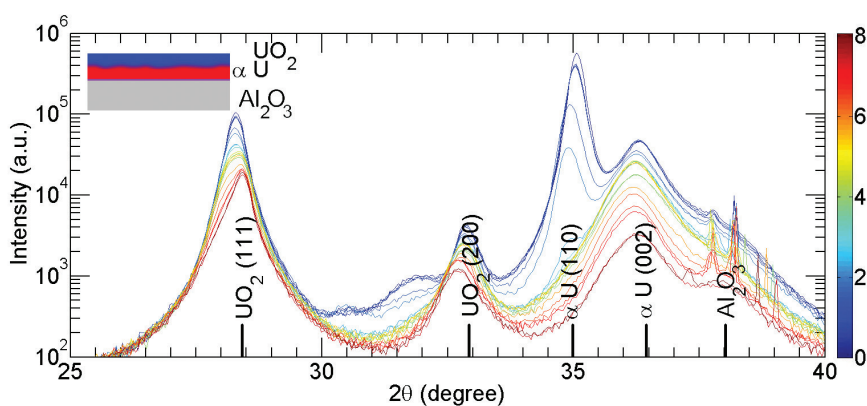


Fig. 18: XRD intensity vs 2θ for the air-grown oxide sample collected with an increasing cumulative hydrogen dose. The colour coding indicated on the right-hand side corresponds to the total accumulative dose (min.bar). Before exposure to air the nominal thickness of U metal was ~ 100 nm. After reaction with air, we estimate that the U metal reduced to 80 nm, with some ~ 60 nm of oxide. The oxide/metal interface is not smooth. The inset in the upper left is a schematic of the sample layer structure.

terminal [2]. The last three phases can produce finely divided, highly reactive (pyrophoric) radioactive powder in the form of UH₃. Generally, a mixture of α -UH₃ and

The bilayers consist of 100 nm of epitaxial α -U (grown on a Nb buffer deposited on sapphire) with a UO₂ overlayer of thicknesses between 20 and 80 nm. The oxides were made

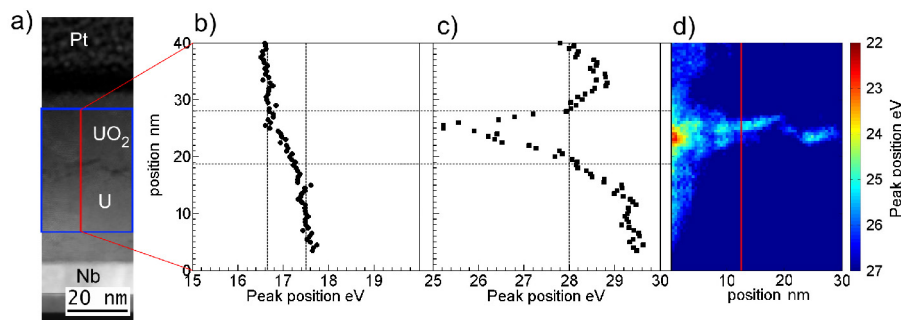


Fig. 19: (a) STEM annular dark field image taken simultaneously with EELS over a 40 nm location range spanning the U-UO₂ interface. Analysis of the uranium P₃ (b) and P₂ (c) edge energy positions highlights three distinct regions: U (between locations 0 and 19 nm), UO₂ (between locations 19 and 28 nm) and UH₃ (between locations 28 and 40 nm). (d) A colour map of the blue region from (a) showing areas where the P₂ edge has been shifted to lower energy suggesting uranium bonding to hydrogen.

- [1] J. Glascott, *Phil. Mag.* 94, 221 (2014).
- [2] R.M. Harker, *J. Alloys Comp.* 426, 106 (2006).
- [3] R. Orr *et al.*, *J. Nucl. Mater.* 477 (Suppl. C) 236 (2016).
- [4] J. Glascott, *Discov. Sci. Technol. AWE*, 6, 27 (2003).
- [5] J.E. Darnbrough *et al.*, *J. Nucl. Mater.* 502, 9 (2018).

For more information contact:
J.E. Darnbrough formerly of School
of Physics, University of Bristol, UK
ed.darnbrough@materials.ox.ac.uk

Using NEXAFS, XPS and TDDFT to probe the electronic structure of ionic liquids

K.R.J. Lovelock, R.M. Fogarty, P.A. Hunt, N.A. Besley, R.A. Bourne, T.W. Chamberlain, P. Thompson

Ionic liquids (IL) are salts composed entirely of mobile cations and anions. Valence electronic structure has a major influence on reactivity [1]. Therefore, IL electronic structure underpins a broad range of potential technologies, including nuclear fuel processing [2] and electrochemical applications (e.g. supercapacitors) [3]. Both Near Edge X-ray Absorption Fine Structure (NEXAFS) spectroscopy and X-ray Photoelectron Spectroscopy (XPS) have historically been used to probe the electronic structure of gases and solids [4]. In particular, ground state oxidation states and atomic charges have been investigated. IL electronic structure has been probed by a number of groups using XPS [5,6] but NEXAFS spectroscopy has not been so widely employed.

NEXAFS spectra were recorded at XMaS at the S K-edge for eight different sulfur-containing IL ions at room temperature. The edge energy, labelled here as E_{NEXAFS} , was determined for each sample. In addition, S K-edge XPS binding energies, E_{B} , were recorded for the same IL selection [7].

As both E_{NEXAFS} and E_{B} can be used to measure sulfur atomic charge, a linear correlation between these values may be expected. Only a rough linear correlation was found between E_{NEXAFS} and E_{B} (Fig. 20); the deviations from linearity were far greater than the experimental error. There are a number of reasons why this lack of linear correlation occurred. In x-ray absorption at the S K-edge, an electron is transferred from the S 1s orbital to an unoccupied orbital, giving rise to an excited state. We used time-dependent density functional theory (TDDFT) calculations to provide detailed insights into the excited states [8]. For the ionic liquid $[\text{C}_4\text{C}_1\text{Im}][\text{NTf}_2]$ the match between the results of TDDFT calculations

for a lone $[\text{NTf}_2]^-$ anion and the S 1s NEXAFS spectrum was excellent (Fig. 21). For the ionic liquid $[\text{C}_4\text{C}_1\text{Im}][\text{SCN}]$ the match between the results of TDDFT calculations for a lone $[\text{SCN}]^-$ anion and the S 1s NEXAFS spectrum was poor (not shown here). By contrast, TDDFT calculations on a $[\text{C}_4\text{C}_1\text{Im}][\text{SCN}]$ ion pair (i.e. two ions) were required to obtain an excellent match to the S 1s NEXAFS [8].

These observations show that the excited states were not always localised on the ion being probed using S 1s NEXAFS spectroscopy. Therefore, NEXAFS spectra contain information on the sulfur atomic charge but also on the identity of the excited states. These different contributions provide an explanation for the lack of a linear correlation between E_{NEXAFS} and E_{B} . Our approach for sulfur-containing IL has since been extended to nitrogen-containing IL [9].

- [1] K. Fukui, *Angew. Chem.-Int. Ed. Engl.* 21, 801 (1982).
- [2] X. Sun *et al.*, *Chem. Rev.* 112, 2100 (2012).
- [3] D.R. MacFarlane *et al.*, *Nat. Rev. Mater.* 1, 15005 (2016).
- [4] D. Briggs & J.T. Grant (eds.) *Surface analysis by Auger and x-ray photoelectron Spectroscopy*, 900 pp (2003). ISBN 1-901019-04-7
- [5] K.R.J Lovelock *et al.*, *Chem. Rev.* 110, 5158 (2010).
- [6] T. Cremer *et al.*, *Chem.-Eur. J.* 16, 9018 (2010).
- [7] R.M. Fogarty *et al.*, *Faraday Discuss.* 206, 183 (2018).
- [8] R.M. Fogarty *et al.*, *Phys. Chem. Chem. Phys.* 19, 31156 (2017).
- [9] R.M. Fogarty *et al.*, *J. Chem. Phys.* 148, 193817 (2018).

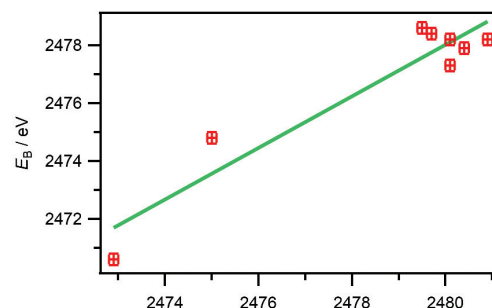


Fig. 20: S K-edge E_{B} against E_{NEXAFS} for eight different ionic liquids.

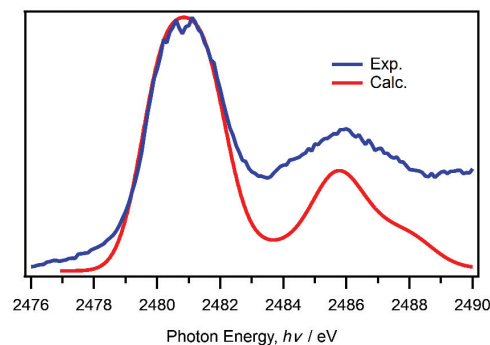


Fig. 21: S K-edge calculated vs. experimental NEXAFS spectrum for $[\text{C}_4\text{C}_1\text{Im}][\text{NTf}_2]$.

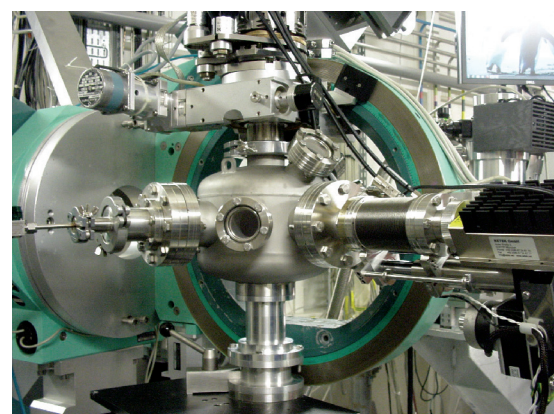


Fig. 22: Spectroscopy chamber used during the experiment with the detector mounted in fluorescence mode.

For more information contact:
K.R.J. Lovelock, Department of
Chemistry, University of Reading, UK
k.r.j.lovelock@reading.ac.uk

ACCESS TO OFFLINE FACILITIES

Our website

This can be found at: www.xmas.ac.uk and contains the definitive information about the beamline and offline facilities, future and past workshops, press articles as well as current Key Performance Indicators (KPIs). You can also follow what happens on the beamline via [Twitter @XMaSBeam](#).

Applications for offline time

Submit your application directly on the XMaS web site: www.xmas.ac.uk Select « XMaS Offline Facilities » and then « Application for Offline Facilities ».

Follow the instructions carefully. Do not forget to load your 1-2 page proposal at the end of the application form. We expect user access to our offline laboratories will be permitted for most of the time during the ESRF dark period but there will be periods where access will be limited. Please contact the local staff to discuss any potential experiments.

XMaS will provide travel and subsistence for only 1 user who will be entitled to €70 per day – the equivalent actually reimbursed in pounds sterling. If more users are needed you will need to make a special case. Successful offline proposals will be run as in-house experiments. Laurence Bouchenoire (bouchenoire@esrf.fr) will complete the safety form with information supplied in your application as well as arrange the site passes and any accommodation that may be required. All our users normally stay in the ESRF guest house or in off-site hotels otherwise. User amenities may also be slightly disrupted during the dark period.

PUBLISH PLEASE!!..... and keep us informed

One of the important XMaS KPIs is the number and quality of publications. We ask you to provide Natacha Borrel (n.borrel@warwick.ac.uk) with the reference and DOI whenever a new paper is published. Alternatively, you can submit the reference of your new publication directly through a form on our web site (<https://tinyurl.com/yelguqdlk>). Please also let us know about other impact generated as a result of XMaS work.

IMPORTANT!

It is important that we acknowledge the support from EPSRC in any publications. When beamline staff have made a significant contribution to your scientific investigation you may naturally want to include them as authors. Otherwise we ask that you add an acknowledgement of the form:

“XMaS is a UK national research facility supported by EPSRC. We are grateful to all the beamline staff for their support.”



XMaS, the UK Materials Science Beamline
ESRF - The European Synchrotron,
71 avenue des Martyrs, CS 40220,
38043 Grenoble Cedex 9, France
Tel: +33 (0)4.76.88.25.80 / xmas@esrf.fr



www.xmas.ac.uk



BEAMLINE PEOPLE

BEAMLINE RESPONSIBLE

Didier Wermeille didierwermeille@esrf.fr in partnership with the Directors, oversees the activities of the user communities as well as the programmes and developments that are performed on the beamline. He is also the beamline Safety Representative.

BEAMLINE COORDINATOR

Laurence Bouchenoire bouchenoire@esrf.fr looks after beamline operations and can provide you with general information about the beamline, application procedures, scheduling, etc. Laurence should normally be your first point of contact.

BEAMLINE SCIENTISTS

Didier Wermeille didierwermeille@esrf.fr
Oier Bikondoa oier.bikondoa@esrf.fr and
Laurence Bouchenoire bouchenoire@esrf.fr
are Beamline Scientists and will provide local contact support during experiments. They can also assist with queries regarding data analysis and software.

TECHNICAL SUPPORT

Paul Thompson pthompso@esrf.fr is the contact for instrument development and technical support. He is assisted by John Kervin jkervin@liv.ac.uk who is based at the University of Liverpool. He provides further technical back-up and spends part of his time on-site at XMaS.

PROJECT DIRECTORS

Chris Lucas clucas@liv.ac.uk and Tom Hase t.p.a.hase@warwick.ac.uk continue to travel between the UK and France to oversee the operation of the beamline. Malcolm Cooper m.j.cooper@warwick.ac.uk remains involved in the beamline operation as an Emeritus Professor at the University of Warwick. Yvonne Gründer yvonne.grunder@liverpool.ac.uk joined the management team at Liverpool to provide additional support. She also oversees impact activities. Natacha Borrel n.borrel@warwick.ac.uk and Julie Clark Julie.Clark@liverpool.ac.uk are the administrators on the project, based in the Department of Physics at Warwick and Liverpool, respectively. Natacha is the point of contact for user T&S claims and co-ordinates the annual XMaS Scientist Experience.